A NOVEL APPROACH TO STRONG GROUND MOTION ATTENUATION MODELING

Vladimir Graizer[1] and Erol Kalkan[2]

[1] *Geophysicist, U. S. Nuclear Regulatory Commission, Washington, DC, USA*
Email: Vladimir.Graizer@nrc.gov
[2] *Structural Engineer-Seismologist, 4728 Donnie Lyn Way, Carmichael, CA, USA*
Email: kalkan76@msn.com

ABSTRACT

Spatial distribution of ground motion data of recent earthquakes unveiled some features of peak ground acceleration (PGA) attenuation with respect to closest distance to the fault (*R*) that current predictive models may not effectively capture. As such, (1) PGA remains constant in the near-fault area, (2) may show an increase in amplitudes at distances of about 3-10 km from the fault-rupture, (3) attenuates with slope of 1/*R* and faster at farther distances, (4) and intensifies at certain distances due to basin effect (if basin is present). A new PGA attenuation model is based on records from shallow crustal earthquakes compiled in the Next Generation Attenuation (NGA) database with a number of additions from recent Californian and worldwide events. A novel feature of the predictive model is its new functional form structured on the transfer function of a single degree of freedom oscillator. In addition, a new PGA-based predictive model was developed for PGV and 5% damped pseudo spectral acceleration (SA) ordinates of free-field horizontal component of ground motion.

KEYWORDS: Response spectrum, Near-field, Ground motion prediction, Site effects, Spectral shape.

1. PREDICTIVE MODEL FOR PGA

Spatial distribution of ground motion data recorded in the proximity of the earthquake fault zones (Parkfield 2004, Imperial Valley 1979, Chi-Chi 1999, Loma Prieta 1989 and Northridge 1994) revealed important attenuation characteristics of PGA with respect to distance from the source as: (1) PGA remains constant in the near-fault area, (2) it exhibits a bump (an increase in amplitude) or a turning point at certain distance (about 3-10 km) from the fault surface, (3) it attenuates with slope of R^{-1} and faster at larger distances, (4) its amplitudes can be amplified at certain distances, for example as a result of basin effect.

The well-known transfer function of a single degree of freedom (SDF) oscillator has analogous characteristics in a way that it remains constant at low frequencies (*f*), attenuates proportionally to f^{-2} at high frequencies and may have a resonance (bump) around the natural frequency, f_0 depending upon damping, D_0. Based on this analogy, a conceptual approach was suggested in which ground motion parameters are treated as an output of cascading filters (with distance *R* being equivalent to square of frequency, f^2), whereby each filter is a mathematical expression used to simulate a certain physical phenomenon (Graizer and Kalkan, 2007). Accordingly, the first filter has a response characteristic with constant level at very short fault distances, a bump or a turning point around R_0 (depend upon magnitude) and a decrease proportional to R^{-1}. The second filter can have two different settings depending upon damping: $D_1 = 0.65$ (no bump) or lower damping D_1~0.40 (with a bump at around R_1). Utilizing second filter with parameter $D_1 = 0.65$ essentially does not affect attenuation of PGA at distances shorter than R_1, and only affects attenuation slope. By lowering the damping parameter this secondary filter can successfully capture basin effect by slightly amplifying ground motions in the near-field and more at distances around R_1. The second settings also result in faster attenuation $R^{-1.5}$ at distances more than the threshold distance R_1. Similar to the basin effect, filter can be tuned to model possible bump on the attenuation curve due to effects similar to reflection from Moho surface at distances of about 50-60 km from the source (Somerville and Yoshimura 1990). Attenuation of seismic waves is a combined effect of geometric spreading, reflection, scattering and

other phenomena. Those complicated processes are in a way "natural filtering" of wave amplitudes. Thus, our approach of using cascading filters in attenuation modeling takes its spirit from this natural process, and each filter acts independently to simulate a certain physical effect. The developed model uses moment magnitude M_W as a magnitude measure (henceforth, referred as M), and closest distance to the fault R (referred as "fault distance") as a distance measure. It is structured on the NGA database (Stewart et al., 2008) with a number of additions mainly from recent California earthquakes. Specifically, almost two thirds of data utilized in this study comes from the NGA data set. This representation resembles the digital signal processing and allows creating a system with desired response. The resultant response in fact is a multiplication of transfer functions of each individual filter accounting for different effects in the arithmetic space. In natural logarithmic space, the attenuation formula can be written as:

$$ln(Y) = ln[G(R)] + ln[G_1(R)] \tag{1}$$

or it can be expanded into the following form:

$$ln(Y) = ln(A) - 0.5ln[(1-\frac{R}{R_0})^2 + 4D_0^{\,2}\frac{R}{R_0}] - 0.5ln[(1-\sqrt{\frac{R}{R_1}})^2 + 4D_1^2\sqrt{\frac{R}{R_1}}] + \sigma_{lnY} \tag{2}$$

where σ_{lnY} is the total standard deviation of the equation. Each estimator parameter (i.e., A (amplification coefficient), D_0, R_0 and D_1, R_1) in Equation 2 is explained next.

1.1. Physical Interpretation of R_0 and D_0

For the SDF oscillator, f_0 refers to the natural frequency. In our attenuation formulation, it corresponds to a corner distance (R_0) where the highest ground motion (bump) or a turning point is observed. R_0 is clearly a function of earthquake magnitude. Based on earthquake data corner distance exibits a linear function of magnitude

$$R_0 = c_4 M + c_5 \tag{3}$$

where c_4 and c_5 are the estimator coefficients. Equation 3 implies that for larger magnitudes, turning point on attenuation curve occurs at farther distances. Certain analogy can also be seen between corner distance and the corner frequency in Brune's model (1970, 1971) where corner frequency depends upon the size of the earthquake.

D_0 is another important parameter and quantifies the intensity of bump on the attenuation curve. Initial findings demonstrate that it is a function of magnitude reaching minimum with D_0 = 0.4 (producing a significant bump) for M 6.0 – 6.5 and being higher at M<5.0 and M>7.0 (much lower or no bump) (Eq. 4)

$$D_0 = c_6 \cos(c_7 M + c_8) + c_9 \tag{4}$$

c_6, c_7, c_8 and c_9 are again the estimator coefficients. Relative level of bump decreases for larger and smaller magnitudes. For magnitudes larger than 7.5, bump saturates.

1.2. Magnitude and fault-style scaling

In the initial stage of analyses, variations in site conditions were not distinguished. This stage is essential to obtain the main tendencies in the attenuation of ground motion. Based on the findings, the following scaling function, $A(M,F)$ is proposed:

$$A(M,F) = [c_1 \arctan(M + c_2) + c_3]\ F \tag{5}$$

where c_1, c_2 and c_3 are the estimator coefficients obtained from nonlinear regression, and F represents scaling due to style of faulting. Scaling factor reflects saturation of amplitudes of ground motion with increasing magnitudes. The scaling function is actually calibrated for 4.9 < M < 7.6. It may need additional adjustment for lower and larger magnitudes.

In this study, style of faulting is considered to be a simple scale factor. According to the results of Sadigh et al. 1997, Campbell and Bozorgnia (in Stewart et al., 2008), reverse-fault events create ground motions approximately 28 percent higher than those from crustal strike-slips. Following this finding, we used $F = 1.00$ for strike-slip and $F = 1.28$ for reverse faults. A limited number of normal fault data points (= 15) in our data set did not allow us to constrain the fault parameter for this particular mechanism, therefore normal fault data points were treated in the same category as strike-slip faulting.

1.3. Shallow site conditions

In the light of available studies (a list of references is given in Graizer and Kalkan, 2007), we adopt linear site amplification that can be formulated in natural logarithmic space as

$$F_{site} = b_v \cdot ln(V_{S30}/V_A) \tag{6}$$

which is the equivalent form of linear site correction expression provided by Boore et al. (1997). In the linear site amplification formula suggested by Boore et al. (1997) $b_v = -0.371$, whereas our estimates yield $b_v = -0.24$. Similar to the results of Field (2000), our attenuation model exhibits less amplification as the V_{S30} decreases compared to stiff site conditions.

1.4. Attenuation equation

Examples of application of the model are shown in Figure 1. Its estimator parameters were found through two-stage regression on compiled dataset that includes 2583 PGA measurements. In the first stage of regression, magnitude and distance dependency on attenuation characteristics were evaluated, while in the next stage site and basin effects were incorporated. The final parameters shown in Figure 2 are valid for magnitude range of 4.5 < M < 7.6 and a distance range up to 200 km considered in this study. The total standard deviation (σ_{lnY}) of predictions was calculated as 0.552 comparable with most recent attenuation relations (Stewart et al., 2008).

1.5. Sediment depth basin effect

Basin effect significantly impacts wave field at distances of 30-50 km and more when deep sedimentary basin is present (Lee et al., 1995; Campbell, 1997). In most cases it is associated with large amplitude surface waves. We model this effect by applying second filter. Similar to the first filter, the transfer function of the second filter is determined by the two parameters: distance R_1 and damping D_1. In this case, R_1 describes the area of bump, and D_1 describes its amplitude (low damping D_1 produces higher amplitudes of bump) (see **G3** in Figure 2). If sediments thickness is low, basin effect can be neglected, and D_1 in this case can be taken as 0.65-0.70 (no bump). Application of the second filter with this value of D_1 results in a change of slope at distances larger than R_1 only. Attenuation function will decay proportionally to $R^{-1.5}$ (unlike R^{-1} decay produced by the **G2** filter in Figure 2).

In general, we envision damping parameter of the second filter (D_1) to be a smooth function of basin depth (thickness of sediment layer). But in our first approximation, we made a simplifying assumption considering basin effect to be the same for all depths of sediments (Z) more than 1 km.

$$D_1 = \begin{cases} 0.65 \text{ for } Z < 1 \text{ km} \\ 0.35 \text{ for } Z \geq 1 \text{ km} \end{cases} \tag{7}$$

In general, we expect D_1 to be decreasing smoothly from 0.7 to 0.3-0.4 and saturating with the increase of thickness of sediments (we plan to study this effect later). The near-field ground motion attenuation is defined by one filter with D_0 and R_0. Damping D_0 describes level of amplification (bump) in the near-field. The first filter describes behavior of the attenuation function up to the distances of about 50 km, and is mostly constrained by earthquake source (magnitude in first approximation). The second filter modifies the behavior of the attenuation function according to the

wave propagation path. It reflects influence of relatively large-scale sediment effects on the attenuation function.

1.6. Comparison with recorded data and attenuation relationships

Prior to comparisons with current attenuation relationships, performance of the proposed attenuation model (Figure 2) is examined through comparisons with actual recorded data. Figure 1 displays comparisons of our predictions with one-to-one correspondence to the actual recorded PGA data from 2 earthquakes. Performance of the attenuation model in predicting the recorded data is tested against four commonly used attenuation relationships of Abrahamson & Silva (1997), Boore et al. (1997), Campbell (1997) and Sadigh et al. (1997). Comparisons with the actual PGA data show that at least for Chi-Chi (M 7.6), Northridge (M 6.7), Imperial Valley (M 6.5) and Parkfield (M 6.0) earthquakes our attenuation curves produce good predictions compared to others (comparisons with other events are given in Graizer and Kalkan, 2007).

2. PGA-BASED PREDICTIVE MODEL FOR SPECTRAL ACCELERATION

Udwadia and Trifunac (1973) demonstrated the correlation between Fourier and response spectra by developing a concept of damped Fourier spectra. This approach shows that the correlation is complex and does not result in approximation of response spectrum with certain mathematical functions. We used empirical approach and found out that the summation of a modified lognormal probability density function [$F_1(T)$] with altered SDF oscillator transfer function [$F_2(T)$] provided the desired shape and also enough flexibility to fit into wide range of spectral shape of real recordings (Figure 3). Each one of these functions simulates certain spectral behavior, for that reason their unification [$F(T) = F_1(T) + F_2(T)$] results in a powerful predictive model (Figure 4). By summing $F_1(T)$ and $F_2(T)$, an approximation function of spectral shape—*SA(T)/PGA*—denoted as SA_{norm} ("*norm*" stands for normalized), is obtained:

$$SA_{norm}(T/M,R,V_{S30}) = I(M,R)e^{-\frac{1}{2}\left(\frac{\ln(T)+\mu(M,R,V_{S30})}{S(M,R)}\right)^2} + \left[\left(1-\left(T/T_{sp,0}\right)^{\zeta}\right)^2 + 4D_{sp}^{\,2}\left(T/T_{sp,0}\right)^{\zeta}\right]^{-1/2} \qquad (8)$$

where $T_{sp,0} = f(M,R,V_{S30})$ is a function of magnitude, distance and site condition. In Figure 3, both $F_1(T)$ and $F_2(T)$ and their summations (*i.e.,* Eq. 8) are plotted against the average spectral shape from the Chi-Chi earthquake. Parameter "ζ" controls the slope of spectral shape decay at long periods. Eq. 8 with $\zeta = 1.0$ results in good match up to period of about 3 seconds, beyond that there is a notable misfit, and average curve is overestimated. This tendency, also observed for other events, is corrected by increasing the order of ζ to 1.5. Faster decay of $\zeta = 2.0$ seems to produce underestimation at long periods (Figure 3). Estimating the slope of attenuation of the response spectrum at long periods may require further studies and more uniformly (from stand point of long-period filter cutoff) processed dataset, because many strong-motion records have been processed with long-period cutoff at 3-5 seconds. Corrected records in the PEER-NGA strong-motion database were processed using 5-pole Butterworth filter at the long-period end and 4-pole Butterworth filter at the short-period end (Stewart et al., 2008). It translates into influence on the long-period region of the response spectra by the data processing procedure (Graizer and Kalkan, 2008).

As shown in Figure 3, average spectrum has different decay before and after its predominant (peak) period. By combining $F_1(T)$ with $F_2(T)$, such difference in slope can be adequately simulated. Function $F_2(T)$ constrains the approximation function to unity at short-period end, and also controls decay at long-periods. $\mu(M,R,V_{S30})$ and $T_{sp,0}(M,R,V_{S30})$ in Eq. 8 collectively identify the location of predominant peak, which is one of the most important shape factor for ground motion spectral shape fit. Likewise, $S(M,R)$ and D_{sp} describe the wideness of the bell-shape together. It is worth emphasizing that Eq. 8 is a continuous function of spectral period, T. Parameters of SA model shown in Figure 4 were computed through nonlinear optimization (Graizer and Kalkan, 2008).

3. PGA-BASED PREDICTIVE MODEL FOR PGV

Our PGV prediction model is set to be a direct function of the PGA attenuation (similar to Campbell, 1997). Thereby, independent parameter effects, well constrained in the PGA attenuation relation, are conveyed to PGV prediction by explicitly utilizing PGA as a scaling factor. The PGV attenuation model in the logarithmic space is represented as:

$$ln(PGV) = d_1 + d_2 M + d_3 \cdot ln(V_{S30}) + d \cdot ln(PGA) + \sigma_{ln(PGV)} \tag{9}$$

where d_1, d_2, d_3 and d are the estimator coefficients obtained through a nonlinear regression, and their optimum values are computed as: d_1 = 1.461, d_2 = 0.656, d_3 = -0.308 and d = 0.732. The standard deviation of prediction ($\sigma_{\ln PGV}$) is found to be 0.570. In lieu of using recorded PGAs, in determination of estimator coefficients, PGA values are retrieved directly from the PGA attenuation model (Graizer and Kalkan 2007). The standard error obtained is similar to the standard error in recent NGA attenuation relations (Stewart et al., 2008).

Both magnitude and soil condition corrections in Eq. 9 are supplementary to those already constrained in the PGA attenuation, and serve to compensate for the residual distribution of PGV predictions with respect to magnitude and soil. Distance effect on PGV attenuation remains analogous to one already constrained in the PGA, thereby no additional scaling parameter of distance is introduced.

4. SUMMARY AND FINAL REMARKS

The proposed PGA attenuation model (referred as GK07-PGA) is structured similar to the transfer function of a SDF oscillator where distance to the fault (R) serves as an equivalent of the square of frequency (f^2). Functional form of the model is composed of a series of filters, each representing a certain physical effect on the attenuation characteristics of seismic radiation. In contrast to the existing attenuation models, our model allows PGA to reach its maximum value at some distance from the fault effectively capturing this phenomenon observed in a number of earthquakes.

An original feature of the proposed *SA* model is its new functional form developed specifically for ground motion spectral shape (*i.e.,* normalized spectrum). Hence, the spectral response ordinates are explicitly computed by anchoring the predicted spectral shape to PGA. Unlike classical spectral attenuation relations, which constitute discrete set of estimator coefficients for each period, the proposed model was designed as a continuous function of period.

The model to predict the response spectrum is based on the GK07-PGA attenuation relation and yields successive predictions of actual spectral shapes in a range of magnitudes from 4.9 to 7.9 within a range of distances from 0 to 200 km, and for various site conditions ($200<V_{S30}<1200$ m/sec). Formulation of response spectrum by a continuous function of period allows calculation of its ordinates at any period of interest within the model range of 0.01 to 10.0 sec (with more confidence up to 5.0 sec because of the limits in the NGA records processing). Similar to the SA predictions, PGV predictions are again based on GK07-PGA model.

Combined attenuation model of PGA, PGV and response spectra presented in this paper is controlled by a number of measurable earthquake and site condition parameters, and represents a complete ground motion prediction model. Compared to the recent NGA relations, the proposed models provide significant ease in both implementation and interpretation of their equation forms as well as controlling physical parameters while providing comparable standard error

REFERENCES

Abrahamson, N. A., and Silva, W. J. (1997). Empirical response spectral attenuation relations for shallow crustal earthquakes. *Seismol. Res. Lett.* **68**, 94-127.

Boore, D. M., Joyner, W. B., and Fumal, T. E. (1997). Equations for estimating horizontal response spectra and peak acceleration from western North American earthquakes: a summary of recent work. *Seismol. Res. Lett.* **68**, 128-153.

Brune, J. (1970). Tectonic stress and the spectra of seismic shear waves from earthquakes. *J. Geophys. Res.,* **75**, 4997-5009.

Brune, J. (1971). Correction. *J. Geophys. Res*., **76**, 5002.

Campbell, K. W. (1997). Empirical near-source attenuation relationships for horizontal and vertical components of peak ground acceleration, peak ground velocity, and pseudo-absolute acceleration response spectra. *Seismol. Res. Lett.* **68**, 154-179.

Field, E. H. (Editor) (2000). Accounting for site effects in probabilistic hazard analyses in Southern California. *Bull. Seism. Soc. Amer.* **90**. 1-244.

Graizer, V. and Kalkan, E. (2007). Ground motion attenuation model for peak horizontal acceleration from shallow crustal earthquakes, *Earthquake Spectra*, **23**, No. 3, 585-613.

Graizer, V. and Kalkan, E. (2008). Prediction of response spectral acceleration ordinates based on PGA attenuation, *Earthquake Spectra* (in press).

Lee, V. W., Trifunac, M. D., Todorovska, M. I. and Novikova, E. I. (1995). Empirical equations describing attenuation of peak of strong ground motion, in terms of magnitude, distance, path effects and site conditions. Report No. CE 95-02. Los Angeles, California. 1-268.

Sadigh, K., Chang, C. –Y., Egan, J.A., Makdisi, F. and Youngs, R. R. (1997). Attenuation relationships for shallow crustal earthquakes based on California strong motion data. *Seismol. Res. Lett.* **68**, 180-189.

Somerville, P.G., and Yoshimura, J. (1990). The influences of critical Moho reflections on strong ground motion recorded in San Francisco and Oakland during the 1989 Loma Prieta earthquake, *Geophys. Res. Letters.,* **17**, 1203-1206.

Stewart, J. P., Ralph J. Archuleta R. J., and Power M. S. (Editors). (2008). Special NGA Issue *Earthquake Spectra*, **24**, No. 1, 1-341.

Udwadia, F. E. and M. D. Trifunac (1973). Damped Fourier spectrum and response spectra. *Bull. Seism. Soc. Am*. **63**, No. 5, 1775-1783.

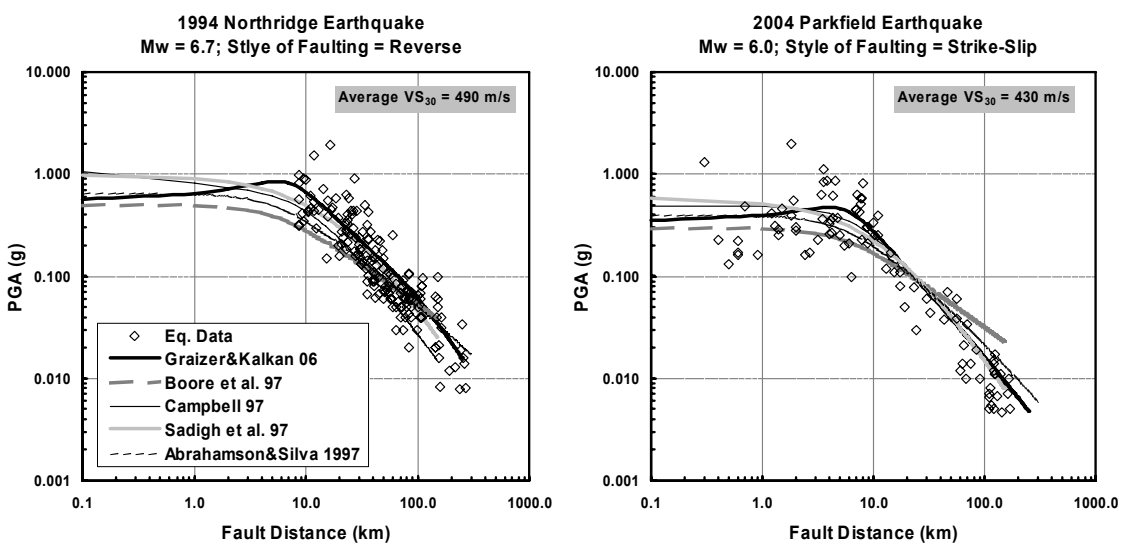

Figure 1. Event-based comparison of our predictions with 1997 attenuation relationships.

PGA = **G1**= Magnitude and Style of Faulting Scaling **x** **G2** =Core Attenuation Equation **x** **G3** = Basin Effect and Long Distance Correction **x** **G4** = Site Correction

$$ln(Y) = \overbrace{ln[A(M,F)]}^{G1} - \overbrace{0.5ln[(1-r_0)^2 + 4D_0^2 r_0]}^{G2} - \overbrace{0.5ln[(1-\sqrt{r_1})^2 + 4D_1^2\sqrt{r_1}]}^{G3} + \overbrace{b_v ln(V_{S30}/V_A)}^{G4} + \sigma_{lnY}$$

where

$$Y = PGA$$

$$r_0 = R/R_0 \qquad r_1 = R/R_1$$

$$A(M,F) = [c_1 \arctan(M + c_2) + c_3]\ F$$

$$R_0 = c_4 M + c_5$$

$$D_0 = c_6 \cos[c_7(M + c_8)] + c_9$$

c_1	c_2	c_3	c_4	c_5	c_6	c_7	c_8	c_9	b_v	VA	R_1	σ_{lnY}
0.14	-6.25	0.37	2.237	-7.542	-0.125	1.19	-6.15	0.525	-0.24	484.5	100	0.552

Note (1): *To capture basin effect it is recommended to set $D_1 = 0.35$, otherwise $D_1 = 0.65$*
(2): *$F = 1.00$ for strike-slip and normal faulting; $F = 1.28$ for reverse faulting*
(3): *R = Closest fault distance and M = Moment magnitude*

Figure 2. GK07-PGA attenuation relation.

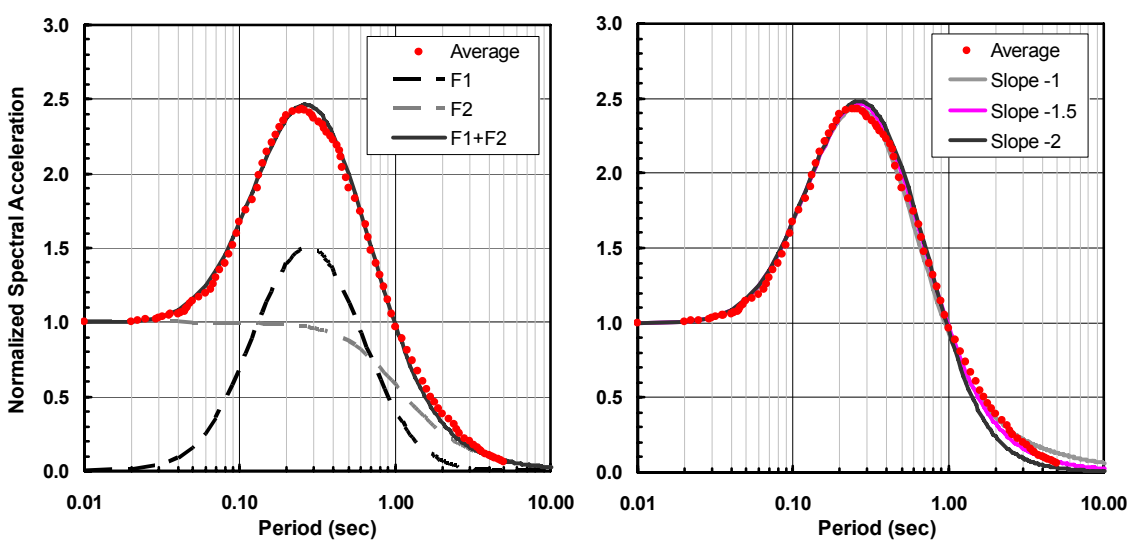

(a) (b)

Figure 3. Approximation function fit to average spectral shape of the 1999 **M**7.6 Chi-Chi earthquake *(Slope of approximation function shown in left-panel is $\zeta = -1.5$).*

$$SA(T) = PGA \times \underbrace{\left(F1(T) = \text{Modified Log Normal Distribution} + F2(T) = \text{Modified SDOF Transfer Function} \right)}_{SA_{norm}(T/M,R,V_{S30})}$$

$$SA_{norm}(T/M,R,V_{S30}) = \overbrace{I(M,R)e^{-\frac{1}{2}\left(\frac{\ln(T)+\mu(M,R,V_{S30})}{S(M,R)}\right)^2}}^{F1(T)} + \overbrace{\left[\left(1-\left(T/T_{sp,0}\right)^{\zeta}\right)^2 + 4D_{sp}^{\,2}\left(T/T_{sp,0}\right)^{\zeta}\right]^{-1/2}}^{F2(T)}$$

R = Closest fault distance

M = Moment magnitude

where

$$\left.\begin{aligned} \mu(M,R,V_{S30}) &= m_1R + m_2M + m_3V_{S30} + m_4 \\ I(M,R) &= (a_1M + a_2)\,e^{a_3R} \\ S(M,R) &= s_1R - (s_2M + s_3) \end{aligned}\right\} \text{Sub-functions of } F1(T)$$

$$\left.T_{sp,0}(M,R,V_{S30}) = t_1R + t_2M + t_3V_{S30} + t_4\right\} \text{Sub-function of } F2(T)$$

m_1	m_2	m_3	m_4	a_1	a_2	a_3	D_{sp}
-0.0012	-0.4087	0.0006	3.63	0.017	1.27	0.0001	0.75

t_1	t_2	t_3	t_4	s_1	s_2	s_3	ζ
0.0022	0.63	-0.0005	-2.1	0.001	0.077	0.3251	1.5

Estimator coefficients

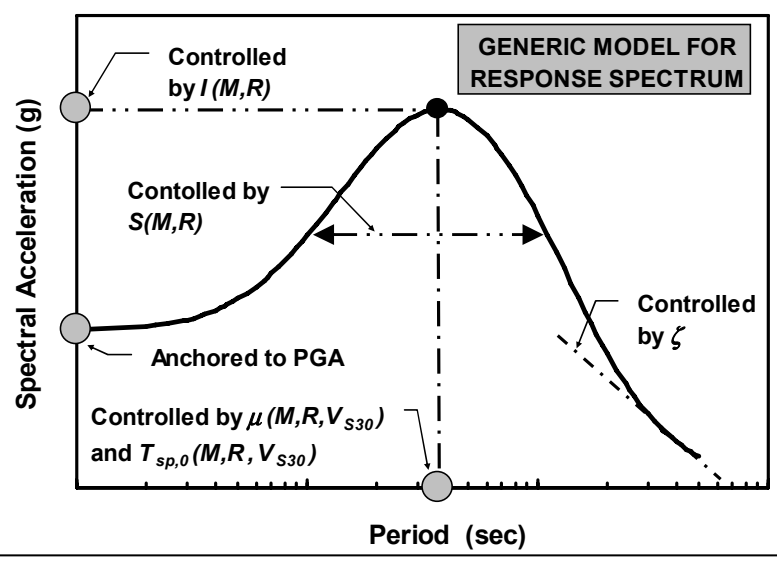

Figure 4. Graizer-Kalkan prediction model for five percent damped response spectral acceleration ordinates.